



Effect of micro-textured morphology with different wettabilities on tool cutting performance

Zengfeng Duan¹ · Ling Chen¹ · Binbin Li¹

Received: 24 January 2022 / Accepted: 9 October 2022 / Published online: 19 October 2022
© The Author(s), under exclusive licence to Springer-Verlag London Ltd., part of Springer Nature 2022

Abstract

Difficult-to-machine materials such as Ni-based superalloy suffer from severe tool wear and poor surface quality; therefore, the cooling mechanism is the key to improving machining performance and reducing the environmental pollution in manufacturing. In the past, plenty of studies verified that the micro-texture on the cutting insert improved the cutting performance under the same cooling condition. The main explanation is that the second generated cracks caused the capillary siphon phenomenon and increased the wettability of the subsurface of the workpiece. In order to investigate the effect of surface wettability differences on the cutting performance of the tool under different micro-textured morphologies, three types of micro-textured CBN tools with pit, linear, and sinusoidal morphologies were fabricated by laser machining technology. Through cutting experiments on Inconel 718 Ni-based superalloy, the cutting force, tool wear, and machined surface roughness of different micro-textured tools were compared and analyzed. The relationship between cutting performance and wettability of different shaped micro-texture was obtained by measuring the contact angle using PT-705B optical angular contact meter. The experimental results show that the presence of surface micro-textures enhances the surface wettability of the tool. It effectively reduces the cutting force and slows down the rake face's wear and the machined part's surface roughness. Compared with other morphologies, sinusoidal micro-textured tools show the best cutting performance. Among the four morphologies of micro-textured tools, cutting performance improvement increases with surface wettability. More generally, these primary findings are consistent with research showing that wettability is critical in micro-texture generation for high-performance machining. The conclusion is very much the key component in future attempts to overcome the assumption of the capillary siphon phenomenon on the subsurface of the workpiece.

Keywords Micro-texture · Contact angle · Surface wettability · Cutting force · Tool wear · Surface roughness

1 Introduction

Ni-based superalloy is a difficult-to-machine material. It has an indispensable role in aerospace and other industries due to the exceptional mechanical properties and resistance to corrosion at elevated temperature [1]. Moreover, CBN tools are widely used in cutting difficult-to-machine materials because of their high hardness and excellent thermal stability. However, in the actual machining process, conventional tools' cooling and lubricating mechanism make the contact area between the difficult-to-machine material and the tool in a state of high temperature, high pressure, and high stress

for a long time. The extremely high cutting force and cutting temperature lead to excessive tool wear, which also seriously affects the machining quality and machining accuracy of the workpiece surface and even causes serious environmental pollution [2, 3].

In the actual cutting process, in order to achieve cooling and lubrication of the machining area, adding lubricant is the most common method. However, the wettability of the lubricant on the machined surface is a crucial factor affecting its effect, which directly affects cutting fluid penetration and interfacial friction properties of the tool-chip interface [4–7]. The design of a reasonable micro-textured morphology on the tool surface can significantly influence wettability. Because of the capillary action of the grooves or stripe patterns in the micro-textures, it will promote the spread or sliding of the droplets in the parallel direction, thereby increasing the wettability of the processed surface

✉ Ling Chen
chenlingscu@scu.edu.cn

¹ School of Mechanical Engineering, Sichuan University, No. 24 South Section 1, Yihuan Road, Chengdu 610065, China

[8]. The change in wettability will affect the speed at which the lubricating oil reaches the cutting area during the cutting process so that more lubricating oil is stored in the micro-textured space, thereby improving the lubrication performance between the tool and the chip and reducing the frictional resistance. Therefore, the micro-textured tool affects the cutting force during the machining process. At the same time, storing more cutting fluid can also achieve a better cooling effect, which can significantly reduce the cutting temperature during processing and reduce the malignant effects of built-up edge on the tool. These mechanisms of surface micro-texture can ultimately achieve the purpose of reducing tool wear, improving cutting performance, and reducing environmental pollution [9, 10].

In recent years, surface micro-structure has been extensively studied in engineering fields related to cutting and machining. Zhang et al. [11] machined micro-groove textures parallel to the leading cutting edge on the tool's rake face and performed comparative turning experiments with conventional tools without surface textures under the action of magnetic nanofluid and magnetic field. The results showed that when the micro-textured tool and magnetic nanofluid were coupled, the cutting force was reduced by 48.6%, and the surface roughness of the machined workpiece was reduced by 49.1%. Wang et al. [12] used a femtosecond laser to machine four micro-textures on the surface of diamond tools, namely, straight groove arrays, concentric textures, circular arrays, and mesh textures, and investigated the effect of different morphological micro-textures on the cutting performance of diamond tools. It was found that the cutting forces and friction coefficients of micro-textured diamond tools, except for concentric textures, were greatly reduced. From the above research findings, it can be found that surface micro-texture does improve the cutting performance of the tool. At the same time, the study of surface wettability is receiving increasing attention. Wang et al. [13] imitated three surface micro-structures including rice leaf, lotus leaf, and snakeskin on a nickel-plated layer, and measured the contact angle of the surface. The results found that the metal surface was similarly hydrophobic. In order to investigate the effect of different dimensional parameters and process zone overlap on wettability, Tej Pratap et al. [14] used high-speed ball ends to mill three different types of micro-textured surfaces with parallel, staggered indentations, and micro-grids, and measured their contact angles to compare the differences in wettability of Ti-6Al-4 V. The results showed that all morphologies enhanced surface wettability and that low spacing, high depth, and overlapping micro-mesh textures in the processed area produced higher wettability.

Although these studies have demonstrated that micro-textures are beneficial for improving machining performance, these studies have focused on simple shape features such as the

array of holes and linear shapes, lacking other typical features such as sinusoidal shapes to analyze for comparison. Furthermore, the cooling and lubrication mechanism is still key for improving machining performance. The current researches on micro-textures have not been analyzed in terms of the cooling and lubrication mechanism of the cutting fluid capillary siphoning phenomenon. In terms of wettability, the study of the wettability of specific regular surface morphologies has become an important content. However, there are currently few reports on this in the field of cutting. Therefore, in this paper, a new sinusoidal micro-textured morphology is proposed for comparison with the more common textured morphology, using CBN tools as the research object. Three surface micro-textures with the same density and different morphology of pit, linear, and sinusoidal shapes are fabricated on the surface of the CBN tool by laser processing technology. And then the experiments of turning Inconel 718 nickel-base superalloy are performed. By measuring the respective surface contact angles to characterize the excellent degree of wettability and comparing cutting forces, tool wear, and the machined part's surface roughness, the effect of surface wettability differences on the cutting performance of tools under different micro-textured morphologies is investigated.

2 Theoretical models

During metal cutting, the friction between the chip and the tool contact area can be expressed as [15]

$$F_f = A_r \tau_c = a_w l_f \tau_c \quad (1)$$

where A_r is the actual tool-chip contact area, τ_c is the friction surface shear strength, a_w is the cutting width, and l_f is the nominal tool-chip contact length.

Figure 1 shows a simplified model of turning. According to metal cutting theory, the three-dimensional cutting force during turning are [16]

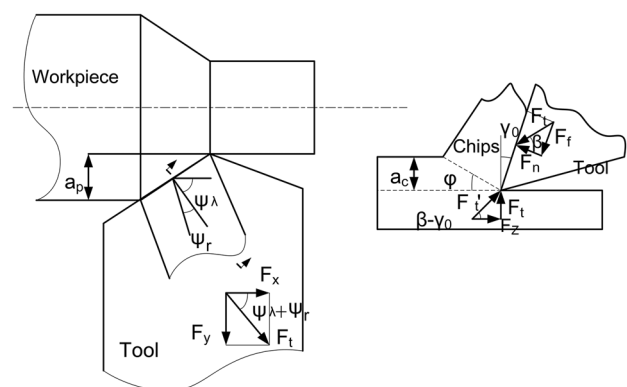


Fig. 1 Simplified model for turning without textured tools

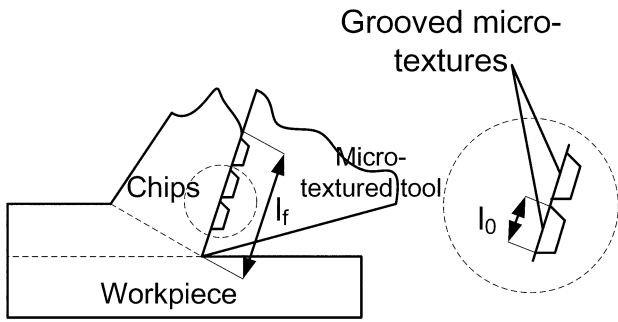


Fig. 2 Simplified model of micro-textured tool cutting

$$F_x = a_w l_f \tau_c \left(\cos \gamma_0 - \frac{\sin \gamma_0}{\tan \beta} \right) \cos (\varphi_r + \varphi_\lambda) \quad (2)$$

$$F_y = a_w l_f \tau_c \left(\cos \gamma_0 - \frac{\sin \gamma_0}{\tan \beta} \right) \sin (\varphi_r + \varphi_\lambda) \quad (3)$$

$$F_z = a_w l_f \tau_c \left(\sin \gamma_0 + \frac{\sin \gamma_0}{\tan \beta} \right) \quad (4)$$

where γ_0 is the tool rake angle, φ_r is the residual deflection angle, β is the friction angle, and φ_λ is the chip flow angle.

Figure 2 shows a simplified model of micro-textured tool cutting. After the micro-texture is processed in the area near the tool tip and cutting edge on the tool rake face, the actual contact length between the tool and chip changes as follows:

$$l'_f = l_f - nl_0 \quad (5)$$

where l'_f is the actual tool-chip contact length, n is the number of textures in the tool-chip contact area, and l_0 is the width of the textures.

So the three-dimensional cutting force after adding the textures is obtained as

$$F'_x = a_w (l_f - nl_0) \tau_c \left(\cos \gamma_0 - \frac{\sin \gamma_0}{\tan \beta} \right) \cos (\varphi_r + \varphi_\lambda) \quad (6)$$

$$F'_y = a_w (l_f - nl_0) \tau_c \left(\cos \gamma_0 - \frac{\sin \gamma_0}{\tan \beta} \right) \sin (\varphi_r + \varphi_\lambda) \quad (7)$$

Fig. 3 Different micro-textured morphologies on the tool surface: (a) pit texture AT, (b) linear texture ZT, and (c) sinusoidal texture XT

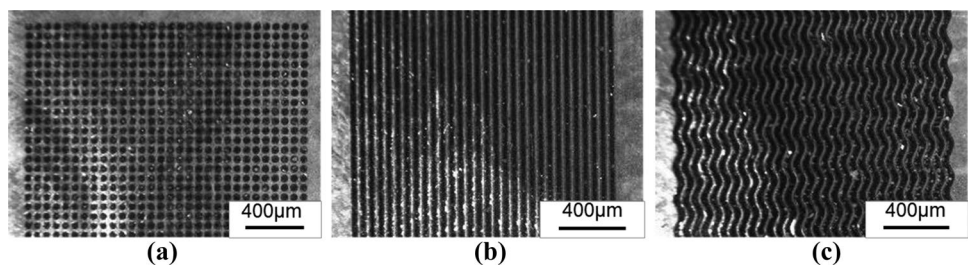


Table 1 CBN tool properties

Young's modulus (GPa)	Poisson's ratio	Coefficient of thermal expansion (m ² /s)	Thermal conductivity (W/m K)	Heat capacity (J/kg K)
720	0.11	4.3×10 ⁻⁶	140	670

$$F'_z = a_w (l_f - nl_0) \tau_c \left(\sin \gamma_0 + \frac{\sin \gamma_0}{\tan \beta} \right) \quad (8)$$

From the above derivation, it can be seen that the placement of the micro-textures reduces the tool-chip contact area and therefore the cutting force.

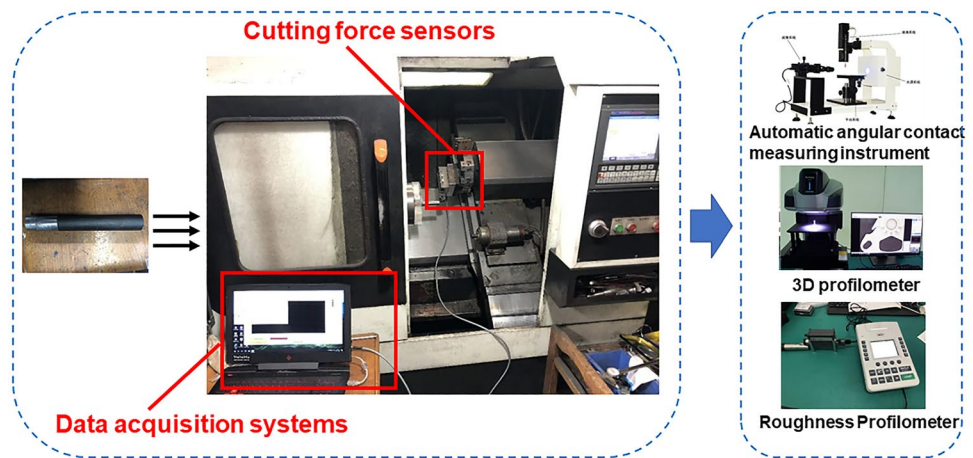
Since micro-texture is a complex surface structure with many morphological structures and complex parametric characteristics, the mechanism of its effect on tool machining performance cannot be easily described by a quantitative and straightforward model. Therefore, in this paper, the texture density of the three micro-textured tools is the same. The contact length of the tool chip is the same, and the purpose of changing the surface wettability is achieved only by changing its morphology. In order to investigate the mechanism of interaction between the properties of surface micro-textures, surface wettability, and cutting forces, and to be able to characterize machining properties by a single indicator of wettability, the following derivation has been made:

After the two extreme cases of Wenzel [17] model and Cassie-Baxter [18] model of solid surface wettability are unified by Bico [19], the equation for the apparent contact angle for wetting at equilibrium can be derived from a practical point of view, which can be extended to obtain the general equations for the apparent contact angle θ_w and the smooth surface intrinsic contact angle θ_0 as follows:

$$\cos \theta_w = \left(f_s + \frac{Ch}{S} \right) \cos \theta_0 + f_s - 1 \quad (9)$$

where S is the total area of an area unit; h is the infiltration depth, in this paper, h is taken to be the near-complete infiltration depth in the texture; C is the total perimeter of the texture of an area unit; and f_s is the percentage of area occupied by solids on the surface of the texture.

Fig. 4 Schematic diagram of the cutting experiment platform



Based on the above parameters and relationships, the relationship model between three-dimensional cutting force and texture surface wettability can be derived when the width, density, and depth of different textures are the same, and the cutting fluid is completely immersed in the texture depth:

$$F_x = \left(\frac{\cos\theta_w - f_s + 1}{\cos\theta_0} - f_s \right) \frac{(l_f - nl_0)P_1}{ch} \quad (10)$$

$$F_y = \left(\frac{\cos\theta_w - f_s + 1}{\cos\theta_0} - f_s \right) \frac{(l_f - nl_0)P_2}{ch} \quad (11)$$

$$F_z = \left(\frac{\cos\theta_w - f_s + 1}{\cos\theta_0} - f_s \right) \frac{(l_f - nl_0)P_3}{ch} \quad (12)$$

where $P_1 = a_w \tau_c (\cos\gamma_0 - \frac{\sin\gamma_0}{\tan\beta}) \cos(\varphi_r + \varphi_\lambda)$, $P_2 = a_w \tau_c (\cos\gamma_0 - \frac{\sin\gamma_0}{\tan\beta}) \sin(\varphi_r + \varphi_\lambda)$, and $P_3 = a_w \tau_c (\sin\gamma_0 + \frac{\sin\gamma_0}{\tan\beta})$.

3 Experiment

3.1 Preparation of micro-textures on tool surfaces

The tool used in the experiment is a CBN tool produced by Zhengzhou Botec, with a specification of 12 mm × 12 mm × 4 mm, which has good wear and heat resistance and can be used for efficient turning of difficult-to-machine materials. The performance parameters of the tool are shown in Table 1. The pit, linear, and sinusoidal micro-textures were machined on the CBN substrate using a fiber laser. The morphology of each structure is shown in Fig. 3. The

micro-textured parameters are as follows: diameter/width 30 μm, edge distance 100 μm, textures spacing 30 μm, depth 30 μm, and sine type amplitude 20 μm. The laser parameters used in the experiment are as follows: laser power 3 W, scanning frequency 600 mm/s, and processing three times. For ease of illustration, the non-textured pitted micro-textured, linear micro-textured, and sinusoidal micro-textured tools are named WT, AT, ZT, and XT, respectively.

3.2 Contact angle measurement

The PT-705B automatic angular contact meter is used to measure the contact angle and thus characterize the wettability of the tool surface, where the software test system supports real-time online measurement of the surface contact angle. The value of the contact angle of a droplet on a solid surface is related to the volume of the droplet and the ambient temperature and humidity, but the four tools in this study are completely the same in material and type except for the textured morphology. Even if the temperature changes, the regularity and trend of their wettability changes are basically the same [20]. The wettability difference between them remains unchanged on the whole, so we can still measure the wettability of tools at ambient temperature to characterize their overall wettability difference. In this experiment, the contact angle was measured at an ambient temperature of 20 °C and a humidity of 63% for droplet volumes of 0.5, 1.0, 1.5, 2.0, and 2.5 μL. The system acquires images every 500 ms for a total of 20 acquisitions and then takes the plural of the acquired data as the contact angle value. The same method was used to measure the non-textured tool and the micro-textured tool in all three morphologies.

Table 2 Main chemical composition of workpiece material (mass fraction percentage)

AL	C	Co	Cr	Cu	Fe	Mn	Mo	Ni	P	S	Si	Ti	V
0.4	0.04	14	19	0.07	18.5	0.5	3	–	0.01	0.01	0.18	0.9	0.5

Table 3 Cutting experimental parameters

Parameters	Conditions
Cooling and lubrication conditions	MQL
Cutting speed	200,000 mm/min
Feed rate	300 mm/min
Cutting depth	0.8 mm

3.3 Cutting experimental equipment and scheme

The turning experiments were carried out on a horizontal CK6136 CNC lathe. The main motor power of the lathe is 5.5 KW, the spindle speed range is 100~2500 r/min, the chuck diameter is 250 mm. The cutting experiment platform is shown in Fig. 4. The workpiece used in this experiment was Inconel 718 nickel-based high-temperature alloy bar stock, 97 mm in diameter. The main chemical composition of the workpiece materials are shown in Table 2.

Turning experiments were carried out on non-textured tools and three shaped micro-textured tools. Table 3 shows the machining conditions. At the same time, a Kistler 9255C three-dimensional cutting force sensor was used to monitor cutting forces in real-time during machining; a VR-5000 3D profile measuring instrument was used to measure the wear on the rake face of the tool. The surface quality was evaluated by the surface roughness value of the workpiece, which was measured using the MahrSurf M300C roughness profilometer. After measuring each machined surface five times in different positions, the data obtained were averaged as the arithmetic mean deviation R_a of the profile.

4 Results and discussion

In this experiment, the surface wettability was characterized by the surface contact angle, which was a minimum of 0° and a maximum of 180° . The smaller the contact angle, the better the wettability of the tool [21]. Figure 5 shows a screenshot of the contact angle tests on four tool surfaces. Figure 6 shows the contact angle magnitudes of different shaped micro-textured tool surfaces at different droplet volumes. As can be seen from the graph, all three shapes of micro-textures can reduce the contact angle and improve the wetting performance of the original surface, but there were

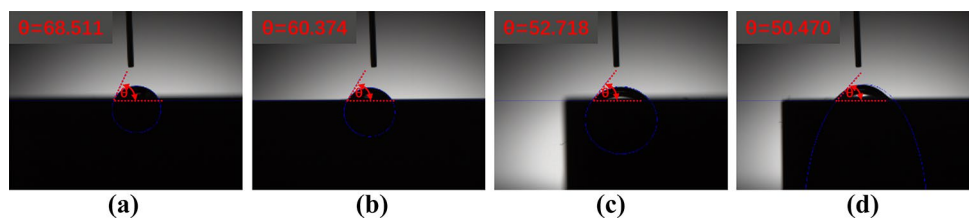
differences between different shapes of textures. The strongest and weakest wettability in this experiment was ranked as sinusoidal, linear, pitted, and non-textured tool. As the droplet volume increases, the contact angle increases and then decreases on the surface of the micro-textured tools for each shape.

From the above equation for the apparent contact angle of immersion under quasi-static equilibrium conditions: $\cos\theta_w = \left(f_s + \frac{Ch}{S}\right)\cos\theta_0 + f_s - 1$, in the four shaped textures with specific rules in this experiment, the solid area percentage was $f_{WT} > f_{AT} > f_{ZT} > f_{XT}$, and the total perimeter of the textures per unit area was related to $C_{WT} < C_{AT} < C_{ZT} < C_{XT}$, while the intrinsic contact angle θ_0 was consistent. After calculations, it was found that the variation in f_s on the three textured surfaces was minimal compared to the variation in C , so the effect of the difference in f_s can be ignored. Thus the following relationship can be obtained: $f_{WT} \approx f_{AT} \approx f_{ZT} \approx f_{XT}$. So it can be concluded that $\cos\theta_w$ and C are theoretically positively correlated, and then there was a relationship: $\theta_{WT} > \theta_{AT} > \theta_{ZT} > \theta_{XT}$. This is consistent with the experimental results.

As shown from Fig. 6, the surface contact angle values appeared to increase and then decrease as the droplet volume gradually increased. This is because the effect of gravity on droplet spreading can be ignored when the droplet volume is small. There are fewer liquid molecules per unit area on the solid surface, and the interaction between liquid molecules is weak. The solid molecules drive the droplet, and the contact angle is small. The contact angle is small and increases as the droplet volume increases. When the droplet volume reaches a certain value, the droplet is driven by gravity to infiltrate into the textures of the surface, and the increase in the solid–liquid area leads to an increase in the solid–liquid adhesion work, resulting in a decrease in contact angle. The internal pressure of the droplet increases as the droplet volume increases, and the internal pressure of the droplet pointing towards the droplet surface drives the droplet to spread around. Therefore, the contact angle decreases as the volume of the droplet increases.

Figure 7 shows the three-dimensional cutting force curve with time for the non-textured tool (WT), the pitted textured tool (AT), the linear textured tool (ZT), and the sinusoidal textured tool (XT). From the graph, it can be seen that the

Fig. 5 Tool surface contact angle measurement: (a) non-texture WT, (b) pit texture AT, (c) linear texture ZT, and (d) sinusoidal texture XT



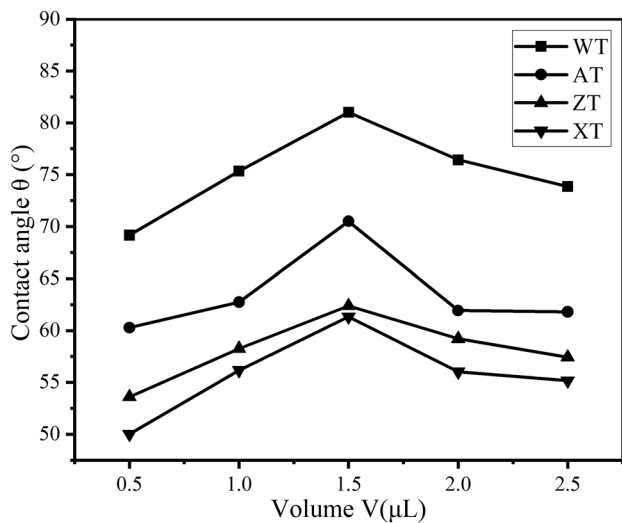
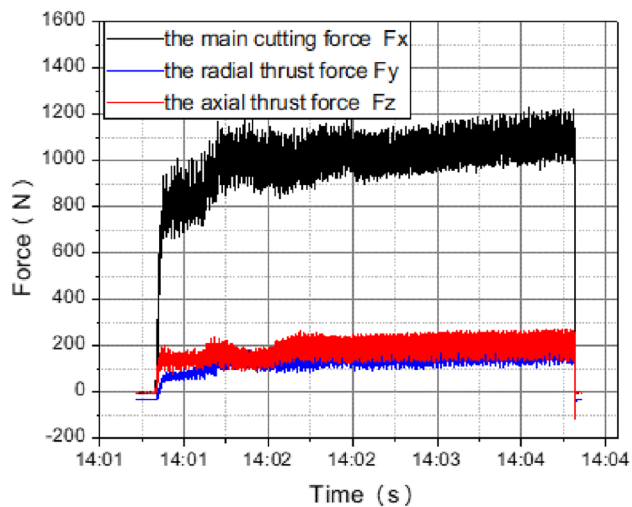


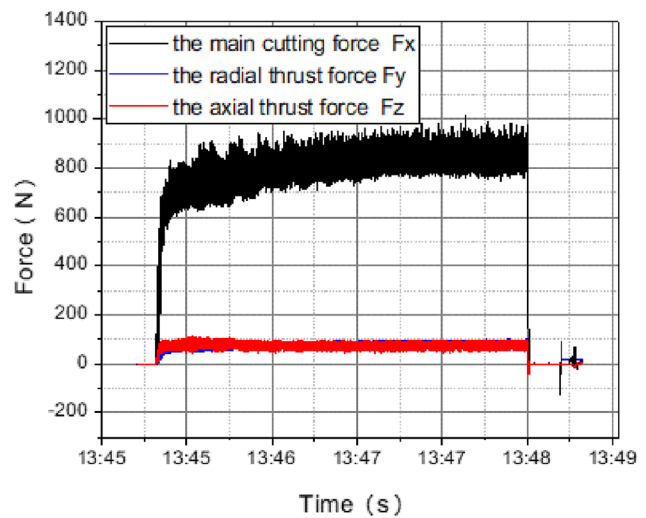
Fig. 6 Surface contact angle at different droplet volumes

three-dimensional cutting force changes were relatively steady for the non-textured tool and the pitted micro-textured tool, while the main cutting force gradually increased and fluctuated more for the linear and sinusoidal micro-textured tools.

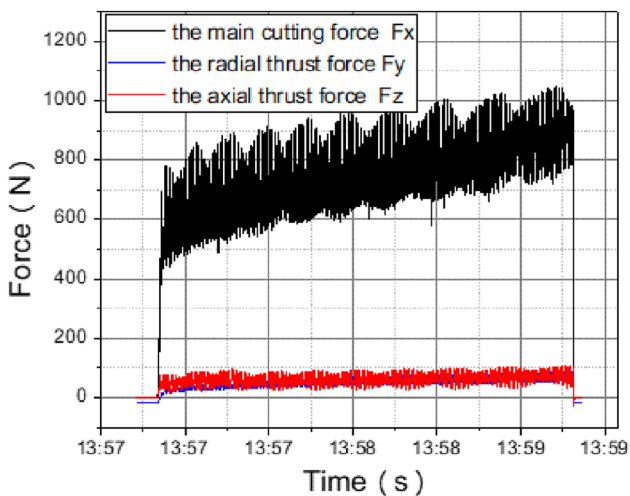
The cutting forces were counted and the average main cutting forces F_x were calculated to be 1051.33 N, 872.41 N, 794.32 N, and 681.45 N for the four tools respectively; the average radial thrust forces F_y were 122.37 N, 81.65 N, 66.74 N, and 53.28 N, respectively; and the average axial thrust forces F_z were 208.93 N, 82.53 N, 77.40 N, and 50.32 N, respectively. Figure 8 shows a comparison of the three-dimensional average cutting forces for the four tools. It can be concluded that under certain cutting conditions, the main cutting forces were reduced by 16.8% for pitted micro-textured tools, 24.5% for linear micro-textured, and 35.2% for sinusoidal micro-textured compared to non-textured tools. The radial thrust forces of all three shaped



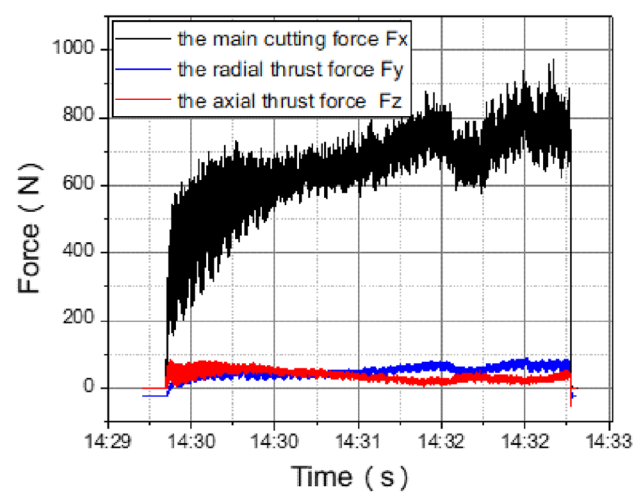
(a)



(b)



(c)



(d)

Fig. 7 Three-dimensional cutting forces: (a) non-textured tool, (b) pitted textured tool, (c) linear textured tools, and (d) sinusoidal textured tools

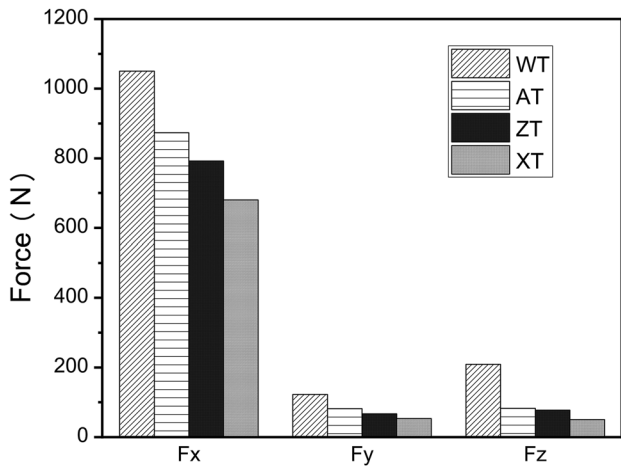


Fig. 8 Comparison of three-dimensional average cutting force of different micro-textures

textured tools were reduced compared to the non-textured tool, by 33.2%, 45.4%, and 56.4%, respectively. The axial thrust forces were reduced by 60.4%, 63.0%, and 75.9%, respectively. In summary, the most significant reduction in cutting forces was found in the sinusoidal micro-textures.

To further investigate the correlation between cutting forces and surface wettability, the average value of the contact angle at droplet volumes of 0.5 μL , 1 μL , 1.5 μL , 2 μL , and 2.5 μL was taken as a measure of wettability. The four tools were 75.168°, 63.451°, 58.177°, and 55.739°, respectively. Figure 9 compares the three-dimensional average cutting forces F_x , F_y , and F_z obtained from cutting experiments and theoretical analysis (Eqs. (10), (11), and (12)) at different contact angles.

As can be seen from Fig. 9, there was a correlation between the cutting forces and the strength of wettability between the

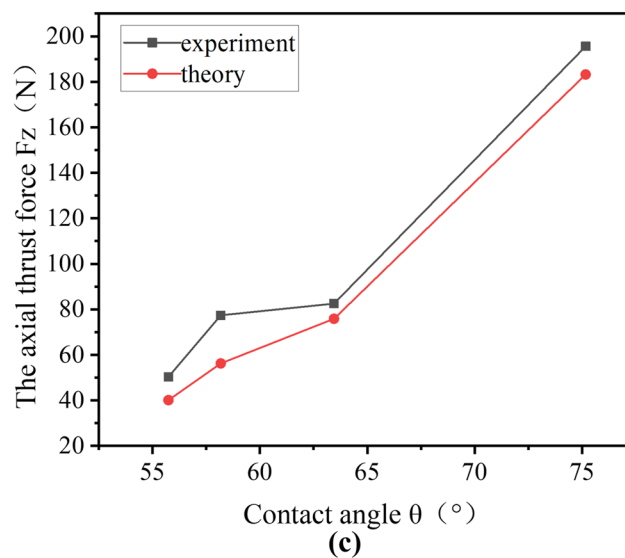
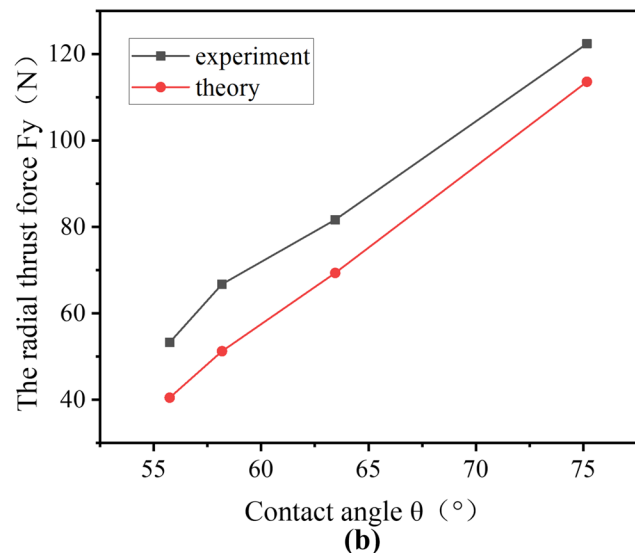
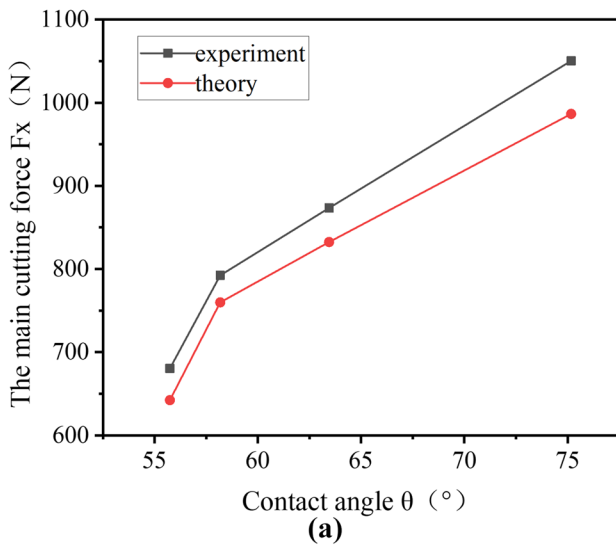


Fig. 9 Cutting forces at different contact angles: (a) F_x , (b) F_y , and (c) F_z

different shaped micro-textured tool surfaces in this experiment. The three-dimensional cutting forces derived from both the theoretical relationship model and experimental measurements increased with increasing contact angle; i.e., the cutting force decreased with increasing wettability. When the contact angle increased from 55.739° to 75.168° , the variation amplitude of the main cutting force was the largest, and the variation amplitude of radial thrust force and axial thrust force was small. The main cutting force F_x values measured by cutting experiments were on average approximately 7% greater than the F_x values derived from the theoretical analysis, the radial thrust force F_y values were approximately 10% greater, and the axial thrust force F_z values were approximately 6% greater. This may be due to the fact that in actual cutting operations, the local capillary interaction between the cutting fluid and the micro-textures results in the infiltration of the cutting fluid not being fully compatible with the theoretical model. In addition, there are various factors such as machine tool vibration and deviations between actual tool geometry and theory that can lead to high cutting forces in actual cutting operations.

The respective wear results were obtained for each tool after cutting 120 mm. Figure 10 shows the wear morphology and wear area width of the rake face after cutting nickel-based alloy with tools under micro-textured morphologies with different surface wettability. As can be seen from the diagram, the tool surfaces all showed some degree of wear, and the most serious wear was found near the tip of the tool. This is because the cutting force and cutting temperature at the tip of the tool is the highest during cutting, so the fracture of the tool base material and the local melting and bonding of the chips are the most serious.

Figure 11 shows the width of the tool wear area at different contact angles. It can be seen that there was a correlation between tool rake face wear and surface wettability, with wear decreasing as tool wettability increased. The most severe wear on the surface of the original tool was $533\ \mu\text{m}$. Compared to the non-textured tool, the width of the wear area was reduced by 13.7% for the pitted textured tool, 40.0% for the linear type, and 52.9% for the sinusoidal type. The non-textured tool with poor wettability and the pitted micro-textured tool had an obvious tool collapse phenomenon. The linear tool collapse area was small, while the sinusoidal micro-textured tool with the best surface wettability was mainly adhesive wear, and there was no tool collapse phenomenon.

The MahrSurf M300C roughness measuring instrument was used to measure the surface roughness of machined parts. For each machined surface, five measurements at different positions were taken and the average value was taken as the arithmetic mean deviation R_a of the machined surface profile. Figure 12 shows the surface roughness values of the workpiece after cutting nickel-based alloys under different

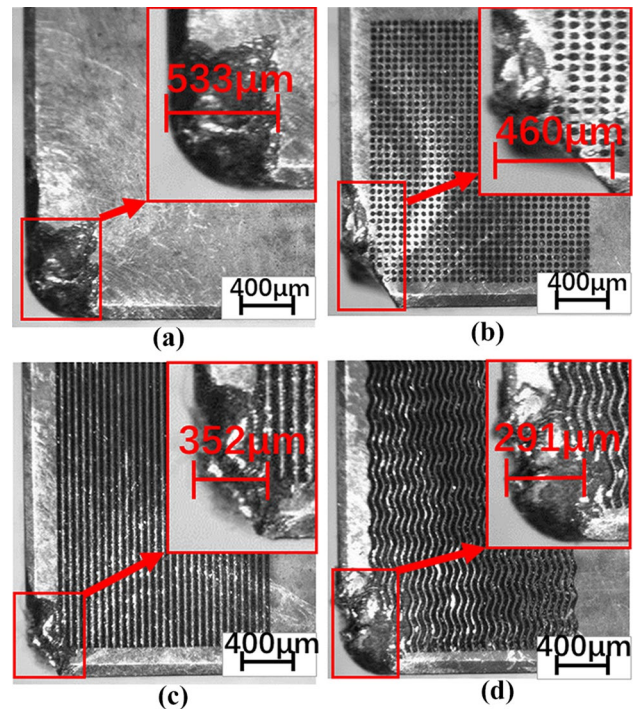


Fig. 10 The wear morphology of rake face: (a) non-textures, (b) pitted textures, (c) linear textures, and (d) sinusoidal textures

surface wettability of the micro-weave morphologies. It can be seen that as the tool wetting performance increased, i.e., the contact angle decreased, the surface roughness value of the workpiece gradually decreased. The reduction in surface roughness of the workpiece under pitted textures was not significant compared to a non-textured tool, with a roughness value of $11.8\ \mu\text{m}$, a reduction of only 7.1%. However, the better wettability of the linear and sinusoidal micro-textured tools showed a better improvement in machining quality, with surface roughness values of $8.5\ \mu\text{m}$ and $6.1\ \mu\text{m}$,

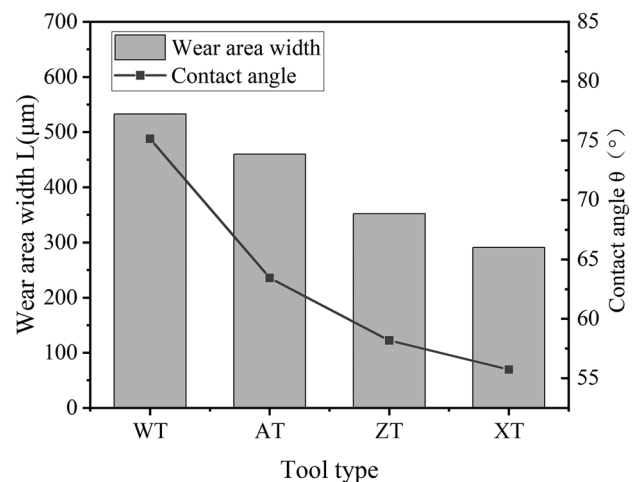


Fig. 11 The wear area width of rake face under different wettabilities

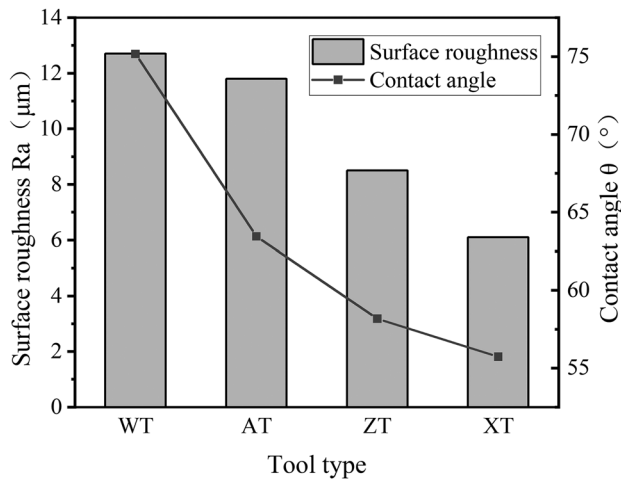


Fig. 12 Tool surface roughness values under different wettabilities

respectively, a reduction of 33.1% and 51.9%, respectively, compared to the non-textured tools.

In the cutting process, the four tool surface micro-textures with specific rules in this experiment had the effect of enhancing the surface wetting properties. The improved wettability would facilitate the penetration of more cutting fluid into the tool-chip interface, thus opening up a cooling and lubrication channel. It can promote lubrication and heat dissipation in the cutting area and reduce frictional resistance between the tool and chip, ultimately reducing three-dimensional cutting forces. So tool wear was also reduced. The improved wetting of the surface resulted in better removal of microscopic chips from the tool-chip sliding friction process, reducing the number of chips that fall on the machined surface, resulting in fewer irregularities in the surface of the workpiece such as pits and scratches, and ultimately improving the surface integrity of the part being machined. The sinusoidal micro-textured tool exhibited the best surface wetting performance in this experiment. Therefore, its cooling and lubrication capacity was the best, and its application in cutting was the most effective in improving the tool's cutting performance. If further experiments can be carried out to investigate the effect of more micro-textures with different parameters and sizes on enhancing surface wettability, and then to reasonably match different cutting parameters and tool-workpiece materials, the tool's cutting performance will be enhanced to a greater extent.

5 Conclusion

In this paper, micro-textured morphologies with different surface wettability were fabricated by laser processing to investigate the effect of differences in wettability on tool

cutting performance. The results showed that among various micro-textured morphologies with the same texture density, the tool's cutting performance and the surface quality of the workpiece improved as the surface wettability increased. The details of the study are as follows:

- (1) The pitted, linear, and sinusoidal micro-textures all increased tool surface wettability, and as the degree of improvement in wettability increased, the degree of reduction in each directional cutting force also increased. Compared to the non-woven tool, the main cutting forces of the three tools were reduced by 16.8%, 24.5%, and 35.2%, respectively. Tool wear was also mitigated. Both the poorly wetted non-textured and pitted micro-textured tools showed significant tool collapse, while the linear type with better wetting had a smaller tool collapse area, and the best wetted positive spin micro-textured tool was in the best condition with essentially no tool collapse. At the same time, the surface roughness of the part being machined was reduced. Among the above tools, the wettability and machining performance of the sine type texture was the best.
- (2) The cooling and lubricating mechanism of the micro-texture was explained from the aspects of drag reduction and the regulation of movement of cutting liquid; that is, the capillary phenomenon exists in the surface micro-texture, which increases the wettability of the machined surface. It promotes more cutting fluid to continue to enter the tool-chip interface, which has a better cooling and lubricating effect. This results in improved friction characteristics and heat dissipation, ultimately improving cutting performance.

Author contribution All authors contributed to the study conception and design. Material preparation, methodology, cutting experiments, writing—original draft, data collection, and analysis were performed by Zengfeng Duan. Validation, investigation, and data curation were performed by Binbin Li. Experimental method guidance and writing—review and editing were performed by Ling Chen. All authors read and approved the final manuscript.

Funding This work was supported by the Key Research & Development Projects (Grant Agreement No. 2020ZDZX0025) of Sichuan Province, China and the Key Research & Development Projects (Grant Agreement No. 22DYF3466) of Sichuan Province, China.

Data availability The datasets generated and/or analyzed during the current study are available from the corresponding author on reasonable request.

Declarations

Ethics approval This article does not contain any studies with human participants or animals performed by any of the authors. Therefore, ethics approval is not applicable.

Consent to participate Consent to participate in this study was obtained from all the authors.

Consent for publication Consent for publication was obtained from all the authors.

Conflict of interest The authors declare no competing interests.

References

- Criado V, Díaz-Álvarez J, Cantero JL, Miguélez MH (2018) Study of the performance of PCBN and carbide tools in finishing machining of Inconel 718 with cutting fluid at conventional pressures. *Procedia CIRP* 77:634–637. <https://doi.org/10.1016/j.procir.2018.08.189>
- Slipchenko K, Petrusha I, Turkevich V, Johansson J, Bushlya V, Ståhl JE (2018) Investigation of the mechanical properties and cutting performance of cBN-based cutting tools with Cr₃C₂ binder phase. *Procedia CIRP* 72:1433–1438. <https://doi.org/10.1016/j.procir.2018.03.180>
- Sheng J, Zhang H, Hu X, Huang S (2020) Influence of laser peening on the high-temperature fatigue life and fracture of Inconel 718 nickel-based alloy. *Theoret Appl Fract Mech* 109:102757. <https://doi.org/10.1016/j.tafmec.2020.102757>
- Tan N, Li Y, Lou L, Zhang G, Xing Z, Wang H (2021) Influence of micro-nano multiscale surface texture on wettability of Ni-based droplets at high temperature. *Surf Coat Technol* 418:127103. <https://doi.org/10.1016/j.surfcoat.2021.127103>
- Divin-Mariotti S, Amieux P, Pascale-Hamri A, Auger V, Kermouche G, Valiorgue F, Valette S (2019) Effects of micro-knurling and femtosecond laser micro texturing on aluminum long-term surface wettability. *Appl Surf Sci* 479:344–350. <https://doi.org/10.1016/j.apsusc.2019.02.025>
- Qin L, Lin P, Zhang Y, Dong G, Zeng Q (2013) Influence of surface wettability on the tribological properties of laser textured Co-Cr-Mo alloy in aqueous bovine serum albumin solution. *Appl Surf Sci* 268:79–86. <https://doi.org/10.1016/j.apsusc.2012.12.003>
- Kubiak KJ, Wilson MCT, Mathia TG, Carval P (2011) Wettability versus roughness of engineering surfaces. *Wear* 271:523–528. <https://doi.org/10.1016/j.wear.2010.03.029>
- Ding Y, Jia L, Yin L, Dang C, Liu X, Xu J (2022) Anisotropic wetting characteristics of droplet on micro-grooved surface. *Colloids Surf A* 633:127850. <https://doi.org/10.1016/j.colsurfa.2021.127850>
- Hao X, Cui W, Li L, Li H, Khan AM, He N (2018) Cutting performance of textured polycrystalline diamond tools with composite lyophilic/lyophobic wettabilities. *J Mater Process Technol* 260:1–8. <https://doi.org/10.1016/j.jmatprotec.2018.04.049>
- Sakthivel G, Sathiya Narayanan N, Vedha Hari BN, Sriraman N, Aanandhamanikandan G, Suraj Nanduru VSP (2021) Performance of surface textured PCD inserts with wettability chemical solutions for machining operation. *Mater Today Proc* 46:8283–8287. <https://doi.org/10.1016/j.matpr.2021.03.252>
- Zhang L, Guo X, Zhang K, Wu Y, Huang Q (2020) Enhancing cutting performance of uncoated cemented carbide tools by joint-use of magnetic nanofluids and micro-texture under magnetic field. *J Mater Process Technol* 284:116764. <https://doi.org/10.1016/j.jmatprotec.2020.116764>
- Wang Q, Yang Y, Yao P, Zhang Z, Yu S, Zhu H, Huang C (2021) Friction and cutting characteristics of micro-textured diamond tools fabricated with femtosecond laser. *Tribol Int* 154:106720. <https://doi.org/10.1016/j.triboint.2020.106720>
- Wang Y, Mo Y, Zhu M, Bai M (2008) Wettability of metal coatings with biomimic micro textures. *Surf Coat Technol* 203:137–141. <https://doi.org/10.1016/j.surfcoat.2008.08.040>
- Pratap T, Patra K (2018) Fabrication of micro-textured surfaces using ball-end micromilling for wettability enhancement of Ti-6Al-4V. *J Mater Process Technol* 262:168–181. <https://doi.org/10.1016/j.jmatprotec.2018.06.035>
- Sun Z, Zhang T, Li P, Wang S, To S, Wang H (2021) Analytical modelling of the trans-scale cutting forces in diamond cutting of polycrystalline metals considering material microstructure and size effect. *Int J Mech Sci* 204:106575. <https://doi.org/10.1016/j.ijmecsci.2021.106575>
- Gupta MK, Korkmaz ME, Sarıkaya M, Krolczyk GM, Günay M, Wojciechowski S (2022) Cutting forces and temperature measurements in cryogenic assisted turning of AA2024-T351 alloy: an experimentally validated simulation approach. *Meas J Int Meas Confederation* 188:110594. <https://doi.org/10.1016/j.measurement.2021.110594>
- Fan Z, Zhao J, Yin J, Hu D, Fu W, Yan H, Song X (2022) Wetting behavior of Al on the surface of SiC textured by nanosecond laser. *Opt Laser Technol* 146:107596. <https://doi.org/10.1016/j.optlastec.2021.107596>
- Du Q, Zhou P, Pan Y, Qu X, Liu L, Yu H, Hou J (2022) Influence of hydrophobicity and roughness on the wetting and flow resistance of water droplets on solid surface: a many-body dissipative particle dynamics study. *Chem Eng Sci* 249:117327. <https://doi.org/10.1016/j.ces.2021.117327>
- Wang F, Cao Z, Liang A, Zhang X, Qiang L, Zhang J (2018) Surface structure and wettability tuning of porous silicon films by capillary-driven surface texturing under different current densities of electrochemical etching. *Mater Lett* 218:249–252. <https://doi.org/10.1016/j.matlet.2018.01.161>
- Al-Ansari S, Wang S, Barifcani A, Lebedev M, Iglauer S (2017) Effect of temperature and SiO₂ nanoparticle size on wettability alteration of oil-wet calcite. *Fuel* 206:34–42. <https://doi.org/10.1016/j.fuel.2017.05.077>
- Yang C, Mei X, Tian Y, Zhang D, Li Y, Liu X (2016) Modification of wettability property of titanium by laser texturing. *Int J Adv Manuf Technol* 87:1663–1670. <https://doi.org/10.1007/s00170-016-8601-9>

Publisher's note Springer Nature remains neutral with regard to jurisdictional claims in published maps and institutional affiliations.

Springer Nature or its licensor (e.g. a society or other partner) holds exclusive rights to this article under a publishing agreement with the author(s) or other rightsholder(s); author self-archiving of the accepted manuscript version of this article is solely governed by the terms of such publishing agreement and applicable law.